Volume 10, Issue 1, 2020, 4752 - 4763 ISSN 2069-5837

Biointerface Research in Applied Chemistry

www.BiointerfaceResearch.com

https://doi.org/10.33263/BRIAC101.752763

Original Research Article Open Access Journal

Received: 02.10.2019 / Revised: 15.11.2019 / Accepted: 17.11.2019 / Published on-line: 21.11.2019

Structural, morphological and electronic properties of cadmium cobalt ferrite nanoparticles

Nehru Boda [1], Kadiyala Chandra Babu Naidu [2], Khalid MujasamBatoo [3], G.Helen Ruth Joice [4], J. Laxman Naik [5], Dachepalli Ravinder [1,*]

[1]Department of Physics, Osmania University, India
[2]Department of Physics, GITAM Deemed To Be University, Bangalore, India
[3]King Abdullah Institute for Nanotechnology, King Saud University, Saudi Arabia
[4]Thiru Kollanjiappar Arts College, India
[5]Department of Physics, University College of Science, Osmania University, India

*corresponding author e-mail address: ***ravindergupta28@rediffmail.com*** | Scopus ID 57190787725

ABSTRACT

Cadmium cobalt ferrite nanoparticles with a chemical formula of $Cd_xCo_{1-x}Fe_2O_4$ (x = 0.0, 0.1, 0.2, 0.3, 0.4, 0.5 & 0.6) (CCF) were prepared via the citrate-gel auto combustion method followed by annealing at 773 Kelvin for 4 hrs in air. Further, the samples were characterized for structural, morphological, elemental, functional group, electrical and thermoelectric properties analysis. The X-ray diffraction patterns showed the single phase cubic structure. The crystalline size of the synthesized Co-Cd ferrites nanoparticle is found in the range of 11 to17 nm. In addition, with an increase of Cd content, we noticed that lattice constants (a) and x-ray density (d_x) values were increasing from 0.8419 – 0.8496 nm and 5.222 – 5.777 g/c.c., respectively. Morphological properties were examined by scanning electron microscopy (SEM) & Transmission electron microscopy (TEM). The tetrahedral (υ_1) and octahedral (υ_2) frequencies were observed at around 400 - 600 cm^{-1}. The electric and dielectric properties such as DC-electrical conductivity (σ_{dc}), dielectric constant (ε'), dielectric loss (ε'') and thermoelectric power parameters were calculated. At a low temperature of 300 K, the samples express the p-type semiconducting nature due to having +ve value of 'S' while the same shows –ve value at high temperature suggesting the n-type semiconducting behavior. Moreover, the magnetic Curie-transition temperatures were determined as a function of composition and noted to be decreasing from 753 – 653 K respectively.

Keywords:*Nanomaterials, Magnetic, Electronic Properties, Dielectrics.*

1. INTRODUCTION

Ferrites having their specialized characteristics like low dc-electrical conductivity and electrical losses...etc, variation at low to high frequencies creates distinguished industrial employment with advanced technology [1]. Specifically, these were quite useful for filters, satellite communication, magnetic tapes, memory devices, electrical components, antenna devices, permanent magnets, soft magnets, humidity sensors, gas sensors, photo catalyst, ferro-fluids, transformer & inductor cores, drug delivery system, actuators, microwave absorbers, magnetic recording media, magnetic hyperthermia treatment, magneto caloric refrigeration, magnetic resonance imaging (MRI), RADAR absorbers, aircrafts, electromagnetic shields etc [1, 2]. However, the nanoferrites were almost confined to microwave device applications (phase shifters, circulators, isolators) because of their considerable low electrical conductivity and dielectric losses at gigahertz frequency range [1, 3]. In nowadays, it has become challenging to control the electrical conductivity at high frequencies. But nevertheless, the efforts have been going on to achieve the required properties. The above quoted applications are remarkably dependent on various factors like synthesis and method of characterization [4, 5].

Ferrites are generally AB_2O_4 (A refers some divalent cations and B indicates Fe^{3+}) spinel structured materials [6, 7]. Several scientists focused on reporting the different properties of these ferrites and ferrite based specimen. Among various researchers, to explain structural, morphological, optical properties and magnetic properties of $CoFe_2O_4$ nanoparticles, Houshiar et al. [8] synthesized and compared physical properties of $CoFe_2O_4$ nanoparticles using different synthesis techniques such as auto combustion, co-precipitation, and precipitation methods. The obtained results evaluated the variation of phase transformation with respect to synthesis techniques.

At most recent, Stein *et al.* [9] synthesized $CoFe_2O_4$ nanoparticles and discussed the superparamagnetic nature of $CoFe_2O_4$ nanoparticles. Besides, the Co-Ni ferrites [10], Li-Co ferrites [11], Co-Cr ferrites [12], Zn-Co ferrites [13], Cd-Co ferrites [1] etc., Studied for the development of electrical and magnetic properties of $CoFe_2O_4$. In the present study, the authors intended to prepare and characterize the Cd-Co nanoferrites via citrate-gel autocombustion method. In fact, this synthesis technique provides more advantages over other methods such as less time & power consumption, relatively low operating temperatures, good homogeneity and inexpensive [11]. It was clear from the literature survey that there very limited investigations were found on electrical and thermoelectric properties of Cd-Co nanoferrites. Therefore, a much attention was carried out to discuss the electrical and thermoelectric properties at length.

2. MATERIALS AND METHODS

The cadmium cobalt nanoferrites (CCF) prepared through citrate gel auto combustion method. The raw materials such as Cadmium Nitrate- 99% pure ($CdNO_3$), Cobalt Nitrate ($CoNO_3$)-99% purity, Ferric Nitrate ($Fe(NO_3)_3 .9H_2O$) with 99% purity,

Citric acid-99.5% Pure ($C_6H_8O_7.H_2O$), and Ammonia solution (NH_3). As per the calculated stoichiometric ratio the chosen nitrates were weighed and dissolved in distilled water to get clear homogeneous solution. The citric acid is used as a fuel due to its good complexing ability from all of the other fuels. The 1:3 ratio maintained for metal nitrate to citric acid in the present synthesis for all the samples, and nitrate-citrate solution was obtained to that ammonia (NH_3) solutions were added drop by drop to maintain pH = 7. The solution of mixer was heated by continuous stirring up to 100^{o}C for 10-12 hours. Then viscous gel was formed. Again water contained mixture was evaporated and it was converted as dry gel and further the internal combustion was taken place. It formed a brown colored product which was a desired sample. The collected ferrite powder was subjected to calcinations at 500^{o}C for 4 hrs and later on, these powders were characterized using few techniques such as X-ray diffractometer (Bruker X-Ray Powder Diffraction Meter, $Cu_{K\alpha}$, λ = 0.15406 nm), Transmission Electron Microscope (TEM: Model Tecnai G20, FEI, USA), Scanning Electron Microscope (Ultra 55 SEM Carl Zeiss), FT-IR spectrophotometer (IR affinity-1, Shimadzu), LCR controller (HIOKI 3532-50), two-probe experiment and thermoelectric measurement for structural, morphological, functional groups, dielectric, dc-electrical conductivity and thermoelectric properties.

3. RESULTS

3.1. XRD analysis.

The X-ray diffraction technique was used in order to confirm single-phase cubic spinel structure formation of CCF nanoparticles as shown in Figure.1. There wereno additional secondary phases were observed. The results obtained from diffraction pattern of $Cd_xCo_{1-x}Fe_2O_4$ (x = 0-0.6) showed the (hkl) values related to the reflection planes (220), (311), (400), (422), (511), and (440) These reflection planes were good agreement with the standard JCPDS card no 52-1798. The average crystallite size was determined using standard Scherrer formula D: $0.9\lambda/\beta Cos\theta$, where β is full width half maxima (FWHM), λ is wavelength of $Cu_{K\alpha}$ source (0.15406 nm) and θ is diffraction angle [14] and the obtained values of crystallite size for synthesized samples were given in Table 1. In the table, the crystallite size was changing from 11 to 24 nm of the various Cd-contents. The variation trend is noted to be almost unsystematic. This is attributed to the unsystematic variation of developed microstrain during the reaction. The lattice parameter (a) of all the synthesized compositions of CCF measured using the formula $a = d\,(h^2 + k^2 + l^2)^{1/2}$ and were given in the Table.1. A plot was drown between the lattice parameter versus cadmium composition and was shown in Figure.2. It was observed that variation of lattice constant with Cd^{2+} content in $Cd_xCo_{1-x}Fe_2O_4$ (x = 0.0-0.6), increased with Cd-content. The increasing of the lattice parameter is observed from 0.8419 – 0.8496 nm as a function of 'x'. This was as a result of cationic replacement by larger ionic radii Cd^{2+} (0.99 Å) in to smaller ionic radii Co^{2+} ions (0.78 Å). This proportional variation indicated that the Co-Cd ferrite system agreement of Vegard's law [7]. Furthermore, with the help of a formula: $d_x = ZM/Na^3$, the theoretical density (d_x) was calculated, where 'Z' is the number of effective atoms per unit-cell, 'M' is the compositional molecular weight, 'N' is Avogadro's number (6.023 x 10^{23}) and 'a' is the lattice constant [12]. The results were listed in Table.1.The Fig.3 showed the behavior of x-ray density (d_x) versus Cd-content. It is noticed that this numerical value is increasing from 5.222 – 5.777 g/c.c. with increase of dopant concentration. The x-ray density (d_x) was depending on the lattice parameter and molecular weight of the sample. From the table, one can observe that molecular weight of the sample was increasing with Cd-content and lattice parameter was also increasing with the increase of Cd-content. This may be due to the larger value of atomic weight of cadmium (112.4 gm/mol) and lesser atomic weight of Fe-(55.9 gm/mol) [16]. The experimental density of the prepared samples was calculated by Archimedes' principle with xylene media using following relation.

$$d_E = \frac{\text{Weight of the sample in air}}{\text{Weight of the sample in air} - \text{weight of the sample in xylene}} \times \text{Density of xylene} \quad (1)$$

The percentage of porosity (P) of the ferrite sample was found using the relation

$$P = \frac{d_X - d_E}{d_X} \times 100 \quad (2)$$

where d_x is the X-ray density &$d_E$is the experimental density. It can be understood that the higher Cd-contents revealed high porosity percentage when compared with low Cd-contents. The results ensured that the porosity of x = 0.4 & 0.5 contents is observed to be ~ 5 % which is higher than the rest of the contents. This may be attributed to the considerable pore content for those compositions. However, during the heating process, the pore fractions will be reduced as a result of the grain growth.

Table 1. Crystalline size (D), Lattice parameter (a), X-ray density (d_x), Expert density (d_E), Porosity (P)

Ferrite Composition	D (nm)	a (Å)	d_x (gm/c.c)	d_E (gm/c.c)	p (%)	υ_1 (cm^{-1})	υ_2 (cm^{-1})
$CoFe_2O_4$	23.78	8.419	5.222	5.351	1.35	570	364
$Cd_{0.1}Co_{0.9}Fe_2O_4$	11.12	8.466	5.253	5.193	1.14	672	382
$Cd_{0.2}Co_{0.8}Fe_2O_4$	14.00	8.468	5.362	5.300	1.15	563	356
$Cd_{0.3}Co_{0.7}Fe_2O_4$	14.62	8.470	5.491	5.394	1.7	561	372
$Cd_{0.4}Co_{0.6}Fe_2O_4$	14.62	8.476	5.584	5.318	4.7	570	381
$Cd_{0.5}Co_{0.5}Fe_2O_4$	14.62	8.485	5.683	5.451	4.1	569	374
$Cd_{0.6}Co_{0.4}Fe_2O_4$	17.82	8.496	5.777	5.619	2.7	559	352

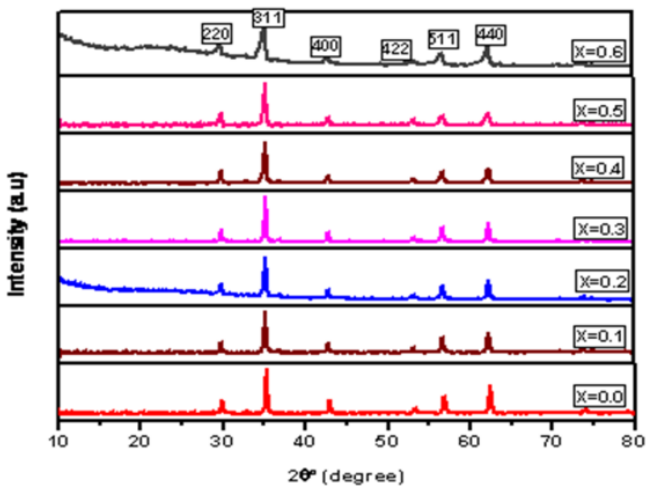

Figure 1. XRD pattern of $Cd_xCo_{1-x}Fe_2O_4$ nanocrystalline ferrites

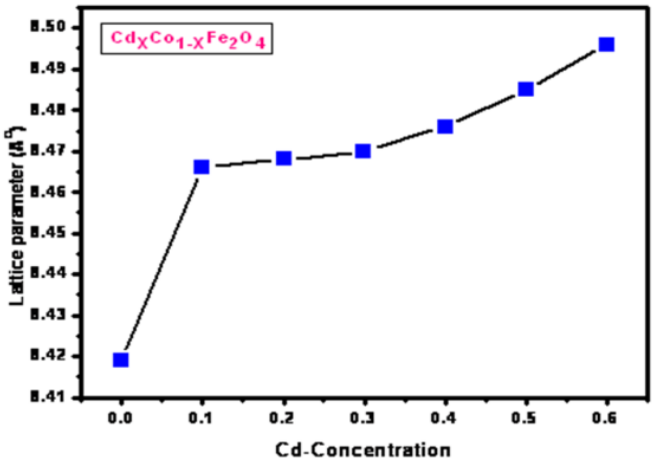

Figure 2. Lattice parameter vs Cd composition

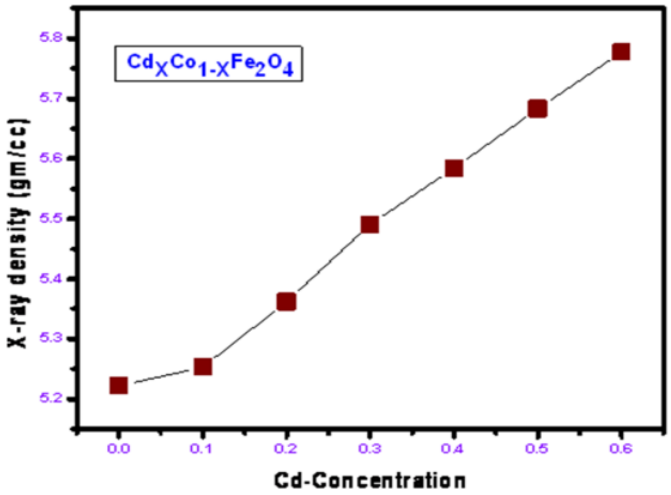

Figure 3. X-ray density vs Cd concentration

3.2. Surface Morphology.

$Cd_xCo_{1-x}Fe_2O_4$ (x = 0-0.6) samples morphology analysis was done by using a scanning electron microscope and Transmission electron microscopy. The micrographs were taken at different magnifications and were shown in Figure.4. All materials revealed the presence of clustered as well as few flat plates like grains. Moreover, the closely associated grains were seen containing agglomeration which may be due to the interaction between the synthesized nanoparticles [4]. The homogeneously distributed grains were noticed for all the nanomaterials. It was also evidenced that x = 0-0.6 samples performed very low pore fraction. Latter, the grain size was observed to be altering from 52 to 150 nm. Further, the hidden elements of the materials were observed using EDS spectra (Fig.5). The indicated spectra of EDS showed existence of Co, Cd, Fe & O elements without any impurities. The morphology was examined using TEM and pictures were shown in Fig.6. It was apparently seen that the x = 0-0.6 compositions showed well defined homogeneous spherical nanoparticles. In addition, the nanoparticles were very close to each other manifesting the agglomeration. The magnetic interactions among the nanoparticles were responsible for this agglomeration. Furthermore, the particle size was observed to be varying from 12 to 68 nm.

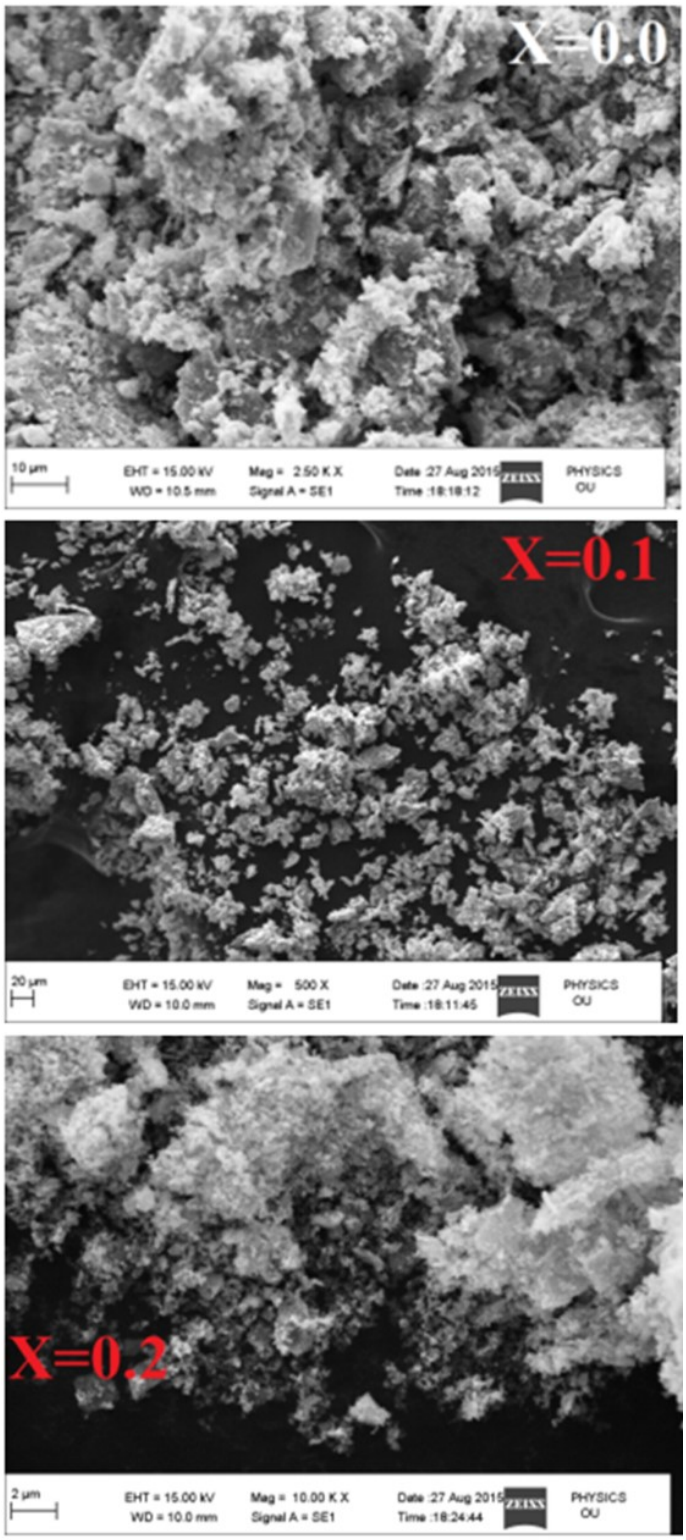

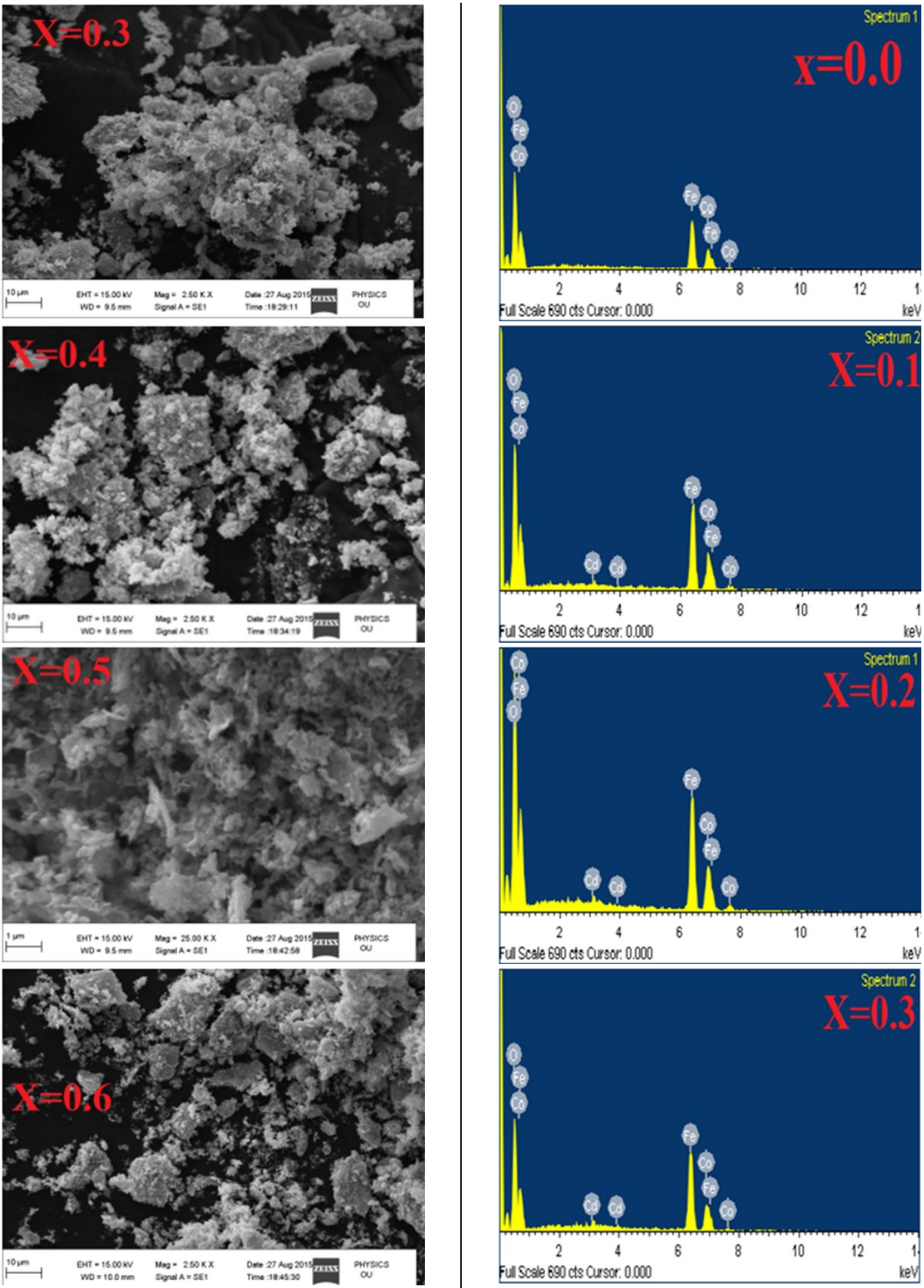

Figure 4. SEM micrographs of $Cd_xCo_{1-x}Fe_2O_4$ ferrites samples at (x=0.0 to 0.6)

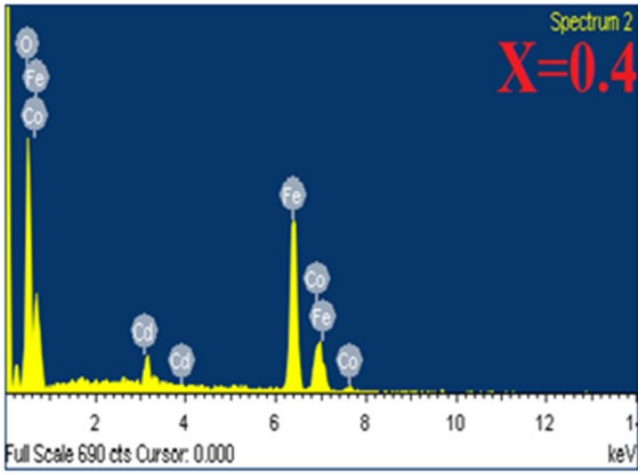

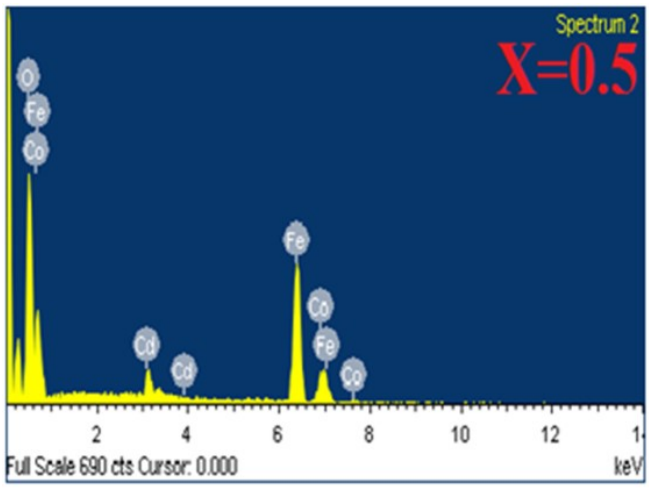

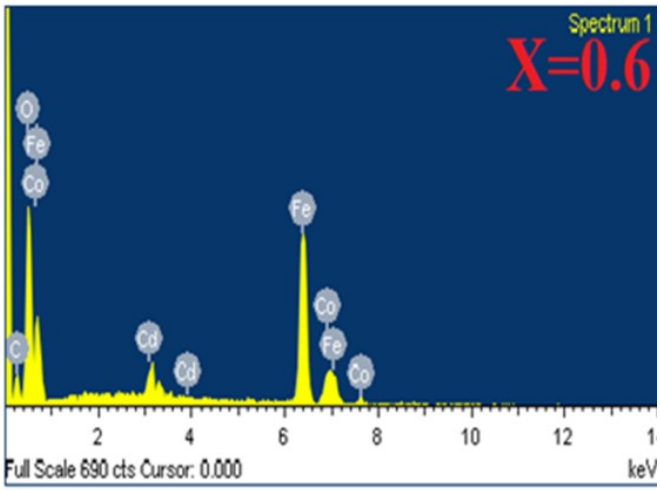

Figure 5.EDS of $Cd_xCo_{1-x}Fe_2O_4$ nano ferrites

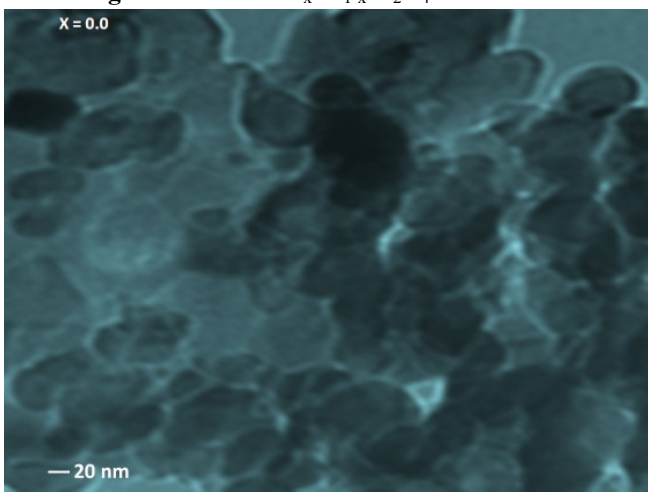

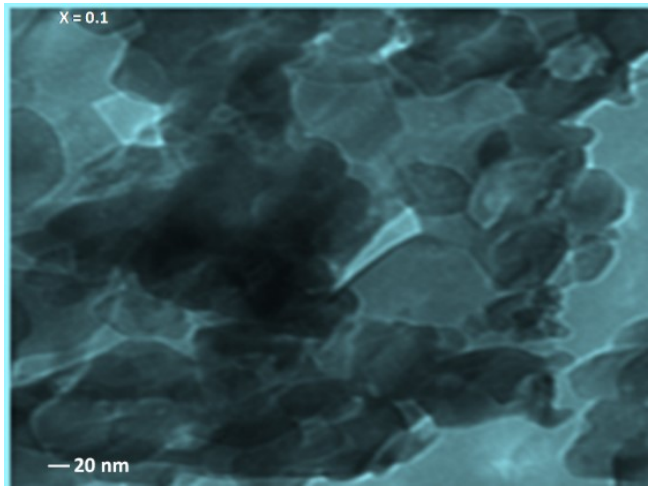

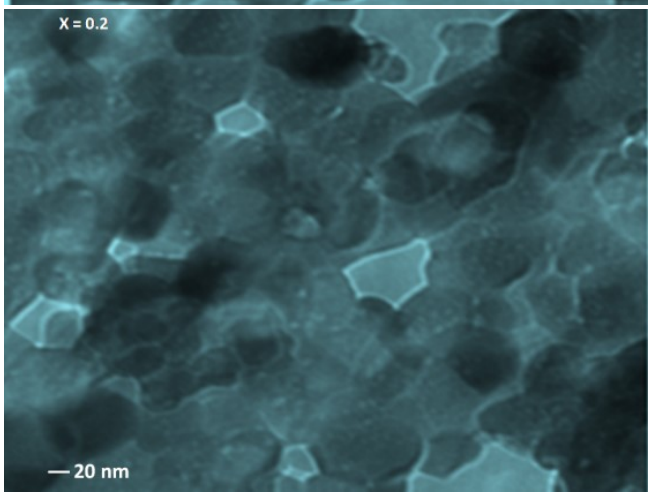

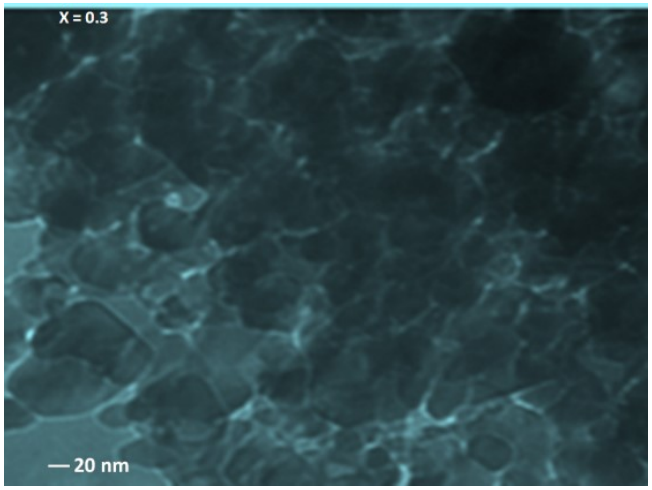

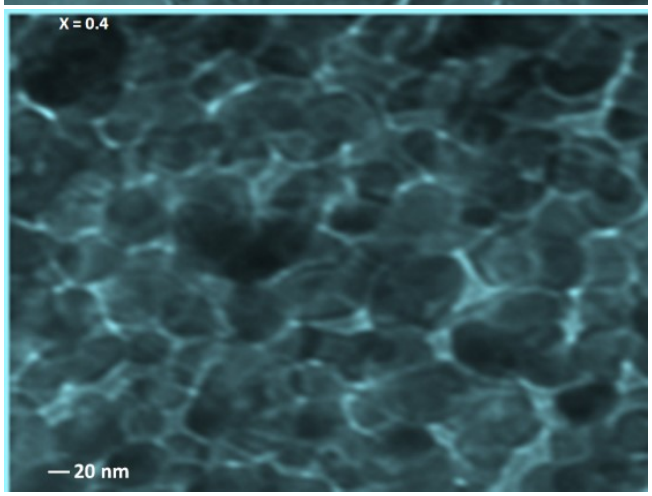

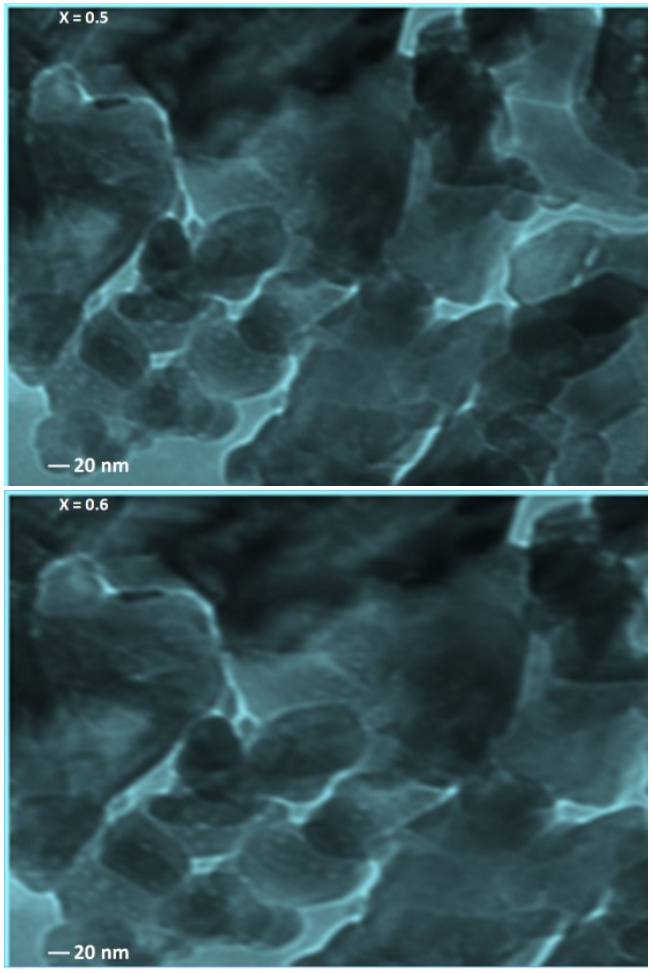

Figure 6.TEM pictures of $Cd_XCo_{1-X}Fe_2O_4$ nanoferrites

3.3. FTIR Spectral Analysis.

The FTIR spectra in Figure.7 cleared the spinel structure with the formation two kinds of characteristic absorption bands found at around 672 cm^{-1} (ϑ_1) and 352 cm^{-1} (ϑ_2). These were associated withthe stretching vibrations of tetrahedral (A-site) and octahedral (B-site) sites respectively. Thus, the formation of single phase cubic spinel structure of ferrites was confirmed [11]. From Figure.7, it was identified that the shifting of band position (600 cm^{-1}) towards lower wavelength region which was due to the increase of Cd^{2+} ions in ferrite and further preferably they may occupy the A-site [12]. However, Co^{2+} ions will have strong preference to occupy B-site [12].

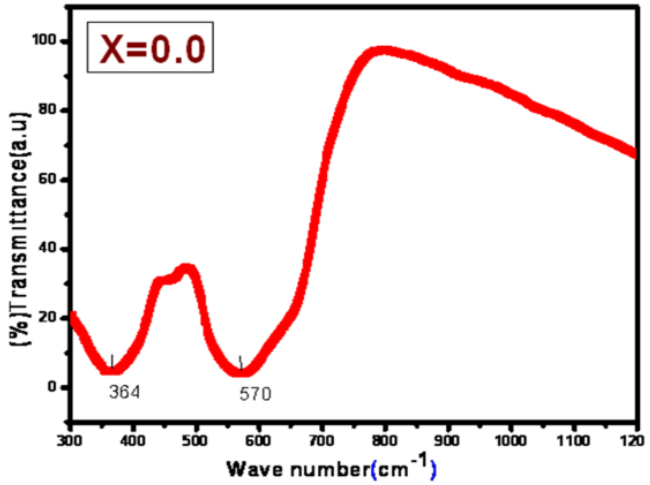

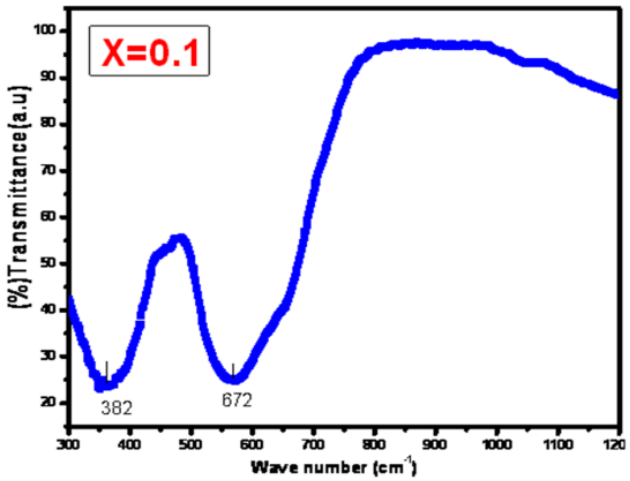

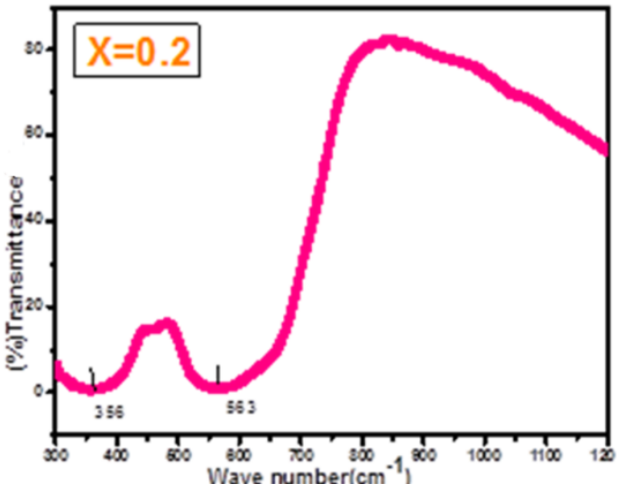

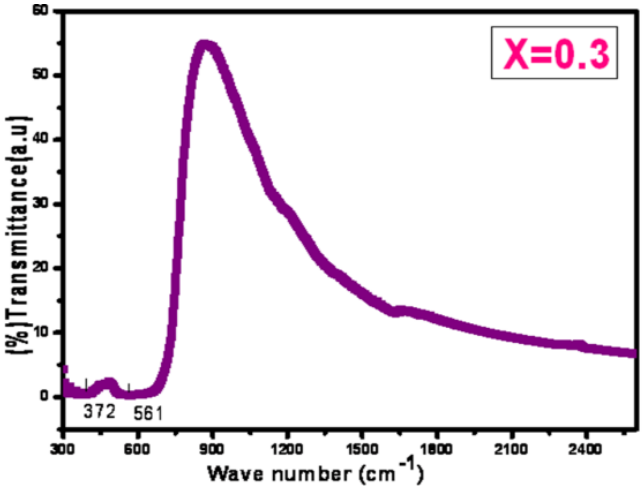

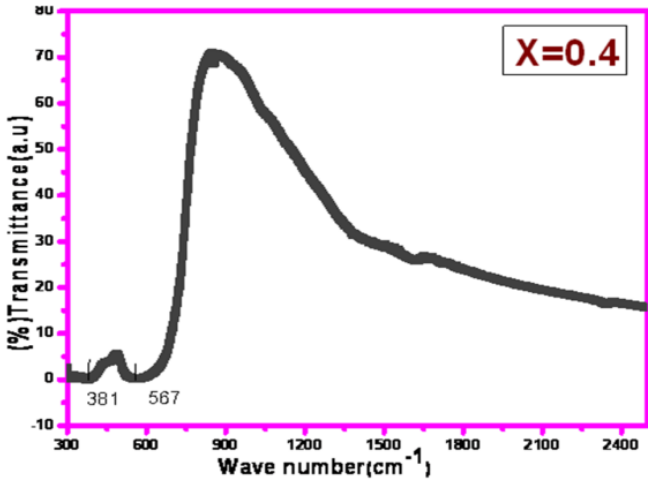

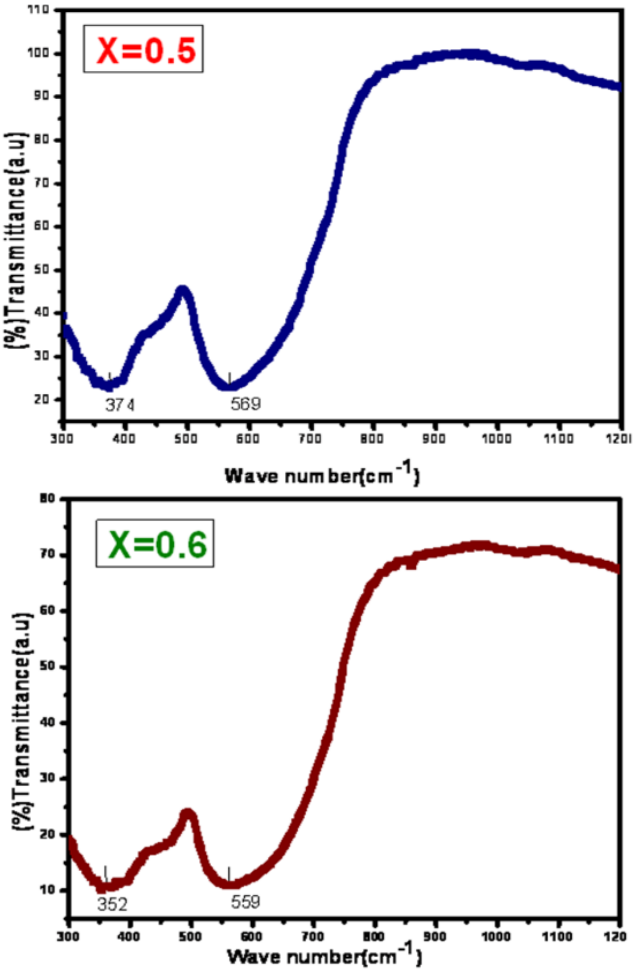

Figure 7.shows FTIR spectra of $Cd_xCo_{1-x}Fe_2O_4$ ferrites samples (x=0.0 to 0.6)

3.4. DC Electrical Properties.

The DC-electrical properties of CCF nanoferrites compositions were studied using two-probe method as a function of temperature from 303 to 953 K. The Fig.8 showed variation of dc-resistivity with temperature for all Co-Cd ferrite samples. The resistivity was decreased with an increase of temperature and therefore confirmed the semiconducting behavior of synthesized Cd-Co ferrite systems. Therefore, the increase of conductivity with increase of temperature upon doping Cd in cobalt nanoferrites from 0.0 to 0.6 was observed in Fig.8. Hence, Verwey and De Boer [17] mechanism used to explain the conduction mechanism in the nanoferrites [18 – 24] which indicated the switch over of electrons between the ions of the same elements present in more than one valence state. The exchange of electrons between $Fe^{2+} \leftrightarrow Fe^{3+}+e^-$ can be responsible for n-type charge carrier and the exchange of holes between $Co^{3+} \leftrightarrow Co^{2+}+e^+$, $Cd^{2+} \leftrightarrow Cd^{1+}+e^+$ will be responsible for p-type charge carriers in the spinel ferrites. It was also observed that the dc-conductivity was increased with increase in Cd^{2+} concentration. This may be explained on the basis of composition of the nanoferrites. In case of Co-Cd nanoferrites, Co^{2+} ions preferred to the octahedral sites, Cd^{2+} ions to the tetrahedral sites and Fe ions to be both octahedral and tetrahedral sites. The temperature dependence of dc-conductivity was plotted using the Arrhenius relation: $\log\sigma_{dc} = \log\sigma_o - (E_a/K_BT)$, where σ_{dc} is the conductivity, σ_o is the conductivity at absolute temperature, K_B is Boltzmann's constant, and T is the temperature [18]. The present nanoferrites performed kink which can be called the Curie temperature. It has evolved due to transition from ferrimagnetic to paramagnetic behavior as shown in Fig.7. From this, it can be understood that the thermal agitation becomes predominant at the transition temperature. Therefore, the charge carriers will respond upto the larger extent. Subsequently, the entropy reaches to the high position. But after crossing the transition temperature, the charge carriers can not respond properly to the applied thermal energy. Thus, the sudden decrease inthe electrical parameters takes place. Furthermore, the activation energies of paramagnetic (ΔE_1) and the ferromagnetic (ΔE_2) blocks were evaluated from the slopes of paramagnetic and ferromagnetic regions using the relation: $\Delta E = 2\times10^{-3}\times$slope [18 - 21]. The observed values are listed in Table.2. It showed that the activation energy was more in the paramagnetic region than in the ferromagnetic region. These were in better agreement with the earlier reports [22]. The transition temperature or relaxation temperatures can be responsible for this kind of change of activation energies. That is, the change of slope of the gradient line takes place before and after transition temperature. In addition, the change of conduction mechanism takes place on either side of T_c. Thus, finally, the ferri to paramagnetic transition occurs. From the Fig. 9, it was concluded that the drift mobility was increased with increase of temperature. This can be attributed to the exchange of thermal energy to the charge carriers after subjecting the nanoferrites to the external temperature. The variation of Curie transition temperature (T_c) as a function of composition was depicted in Fig.10. It was seen in the plot that the T_c was found to be decreasing from 753 to 653 K with increase of Cd. This kind of manner was achieved as a result of the reduction of magnetic exchange interactions between the cations at octahedral site [12].

Table 2. Data on Curie temperature (T_c) and Activation energy (eV)

Sample	Curie Temp (K)	Activation Energy (eV)	
		Para magnetic ($\Delta E1$)	Ferro magnetic ($\Delta E2$)
$CoFe_2O_4$	753	0.628	0.619
$Cd_{0.1}Co_{0.9}Fe_2O_4$	723	0.729	0.678
$Cd_{0.2}Co_{0.8}Fe_2O_4$	713	0.736	0.733
$Cd_{0.3}Co_{0.7}Fe_2O_4$	693	0.801	0.716
$Cd_{0.4}Co_{0.6}Fe_2O_4$	673	0.826	0.761
$Cd_{0.5}Co_{0.5}Fe_2O_4$	663	0.895	0.713
$Cd_{0.6}Co_{0.4}Fe_2O_4$	653	0.911	0.865

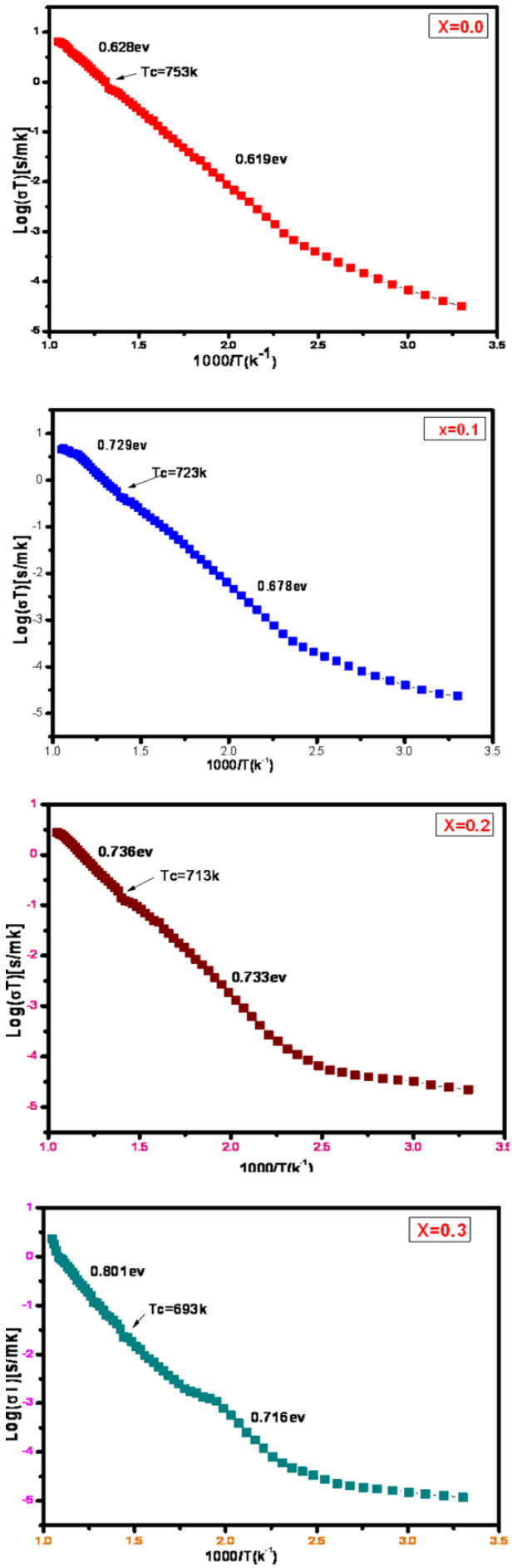

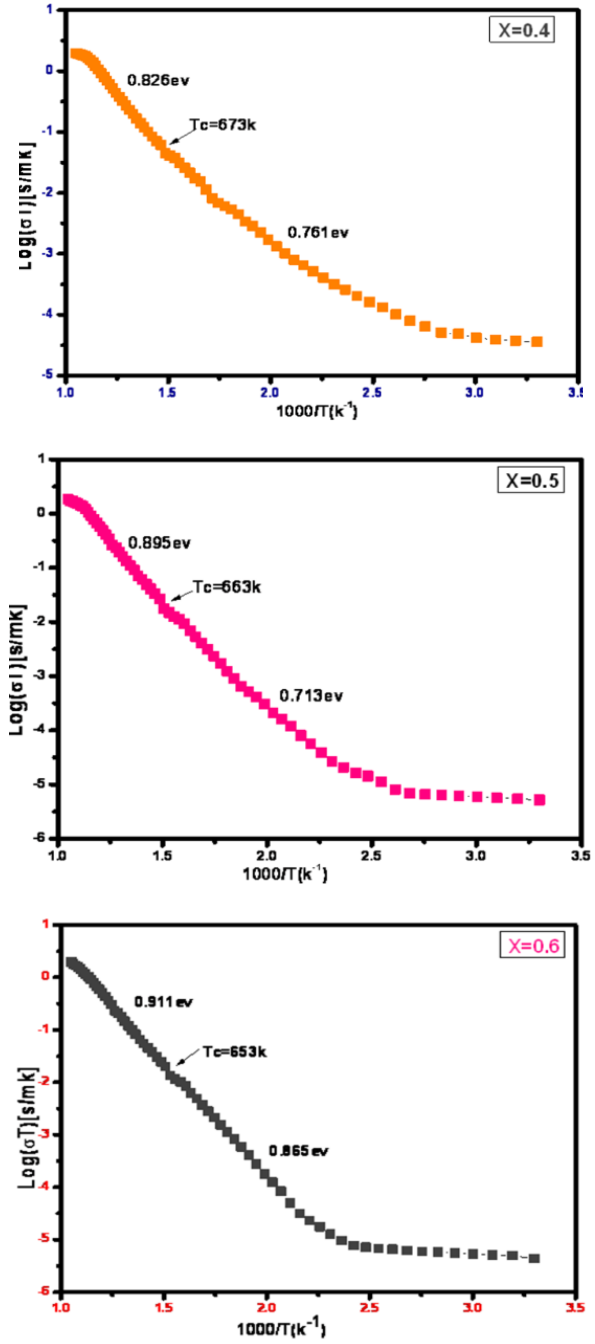

Figure 8. Variation of dc-conductivity with temperature of $Cd_xCo_{1-x}Fe_2O_4$ (x=0.0 to 0.6) ferrites

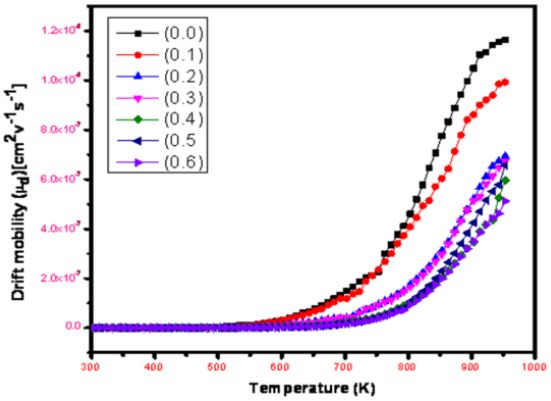

Figure 9. Variation of Drift mobility with temperature of $Cd_xCo_{1-x}Fe_2O_4$ (X=0.0 to 0.6)

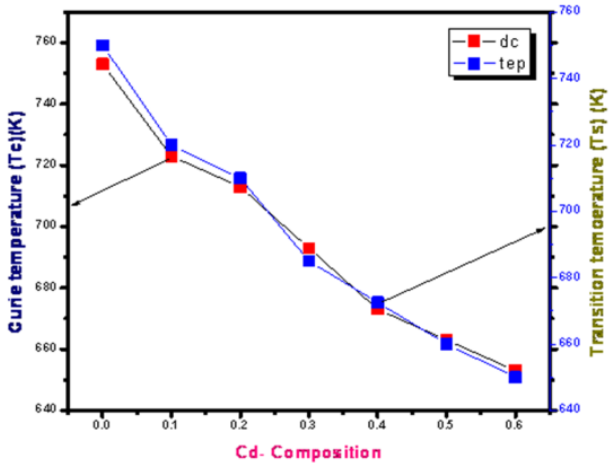

Figure 10. Variation of Curie temperature and Transition temperature with Cd content

3.5. Dielectric Properties.

In general, the dielectric behavior of a material mainly depends on the method of preparation, sintering temperature, sintering time and strength of electromagnetic interactions between constituent phases and structure of phase [11, 12]. The behavior of dielectric parameters was investigated in the range of applied frequency range of 50 Hz to 5 MHz at room temperature. The frequency dependence of real part of dielectric constant (ε') and imaginary part dielectric constant (ε'') at room temperature as shown in Fig.11. The plots revealed that the ε' and ε'' were decreasing exponentially with the increase of frequency. It was normal dielectric behavior. In general, the polycrystalline materials were supposed to consist of two layers such as grain and grain boundary. These may take part in obtaining the trend of dielectric constant (ε') and loss (ε'') as a function of frequency. However, it was an established fact that the grain boundaries can be more resistive layers while the grains can be of low resistive layers [4, 5]. At low input frequencies the charge carriers can respond actively and further they will accumulate at the grain boundary interface. Therefore, huge amount of polarization can be developed. It can be treated as space-charge polarization. This may in turn responsible for the achieved maximum values of dielectric constant and loss at small frequencies [5]. On the other hand, at high frequencies, the efficiency of space-charge polarization becomes diminished and hence it resulted in acquiring the small values of ε' and ε'' at high frequencies. Similar kinds of observations were seen in the literature [4].

3.6. Thermo-electric Properties.

The behavior of Seebeck coefficient ($S = \Delta V/\Delta T$) with temperature of the prepared Co-Cd nanoferrites was shown in Fig 12. It was observed that all the samples revealed similar thermal variation with Seebeck coefficient. The 'S' was increased with an increase in the temperature up to a specific temperature called transition temperature (T_c). However, above the T_c, the 'S' value was further reduced. At small T-values, +ve value of 'S' expressed p-type semiconducting nature of the prepared ferrite samples. Initially, Co-ferrite acted like p-type semiconductor at room temperature (300 K). With increasing of the temperature and Cd-content, the seebeck coefficient was also found to be increased. Above the transition temperature, the seebeck coefficient start decreased with increase in temperature. Then sample behavior was changed to n-type semiconductor behavior [12]. The probable conduction mechanisms in the spinel nanoferrites system under investigation were $Fe^{2+} \leftrightarrow Fe^{3+} + e^-$ (n-type or electron exchange mechanism) [12].

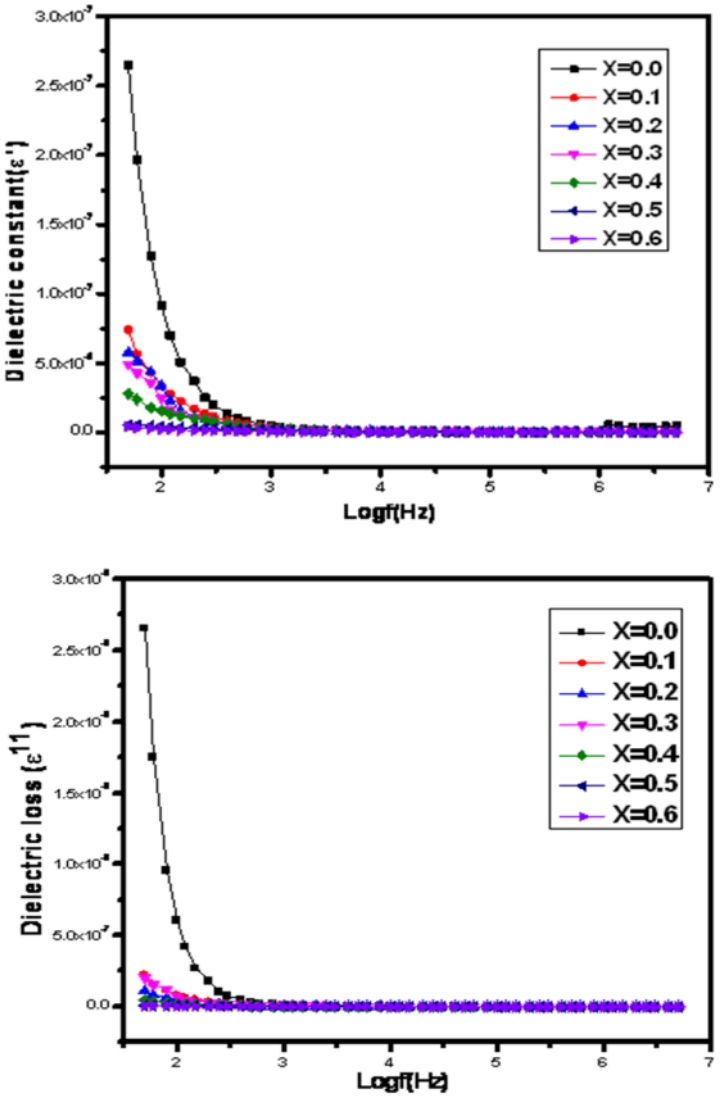

Figure 11. Variation of (a) ε' and (b) ε'' with frequency

In the similar fashion, as the hole exchange is higher than that of electron exchange, subsequently, the p-kind of semiconducting nature can be observed. The converse also becomes true usually. However, as the temperature was increased the larger number of electrons were generated which can lead to n-type semiconducting nature at large temperature values. This evidenced a fact that the samples performed the p-type and n-type semiconducting trend at low and high temperatures respectively. In addition, it was observed that the 'S' value of Co-Cd nanoparticles was increased with increase intemperature. This also evidenced that the more number of n-type charge carriers were developed as a function of temperature. But, a knick was found at specified temperature termed as Curie transition temperature (As shown in Fig.12). As depicted in Fig.12, one can understand that the T_c values of the present materials were diminished as a function of Cd-content. The results were reported in Table 3. The 'S' value was noted to be increasing with Cd-content (Table.3) at room temperature.

Table 3. Shows Transition temperature (Ts), Curie temperature (Tc), DC-conductivity (σ_{dc}) at room temperature, and seebeck coefficient (S)

Composition	Ts (K)	Tc (K)	S (mV/K)	σdc (Ω-1/cm)
CoFe2O4	750	753	-0.06	2.32×10-07
Cd0.1Co0.9Fe2O4	720	723	-0.15	2.61×10-06
Cd0.2Co0.8Fe2O4	710	713	-0.25	7.26 ×10-08
Cd0.3Co0.7Fe2O4	685	693	-0.37	7.36 ×10-08
Cd0.4Co0.6Fe2O4	672.5	673	-0.48	8.92 ×10-08
Cd0.5Co0.5Fe2O4	660	663	-0.51	1.71 ×10-08
Cd0.6Co0.4Fe2O4	650	653	-0.62	1.43 ×10-08

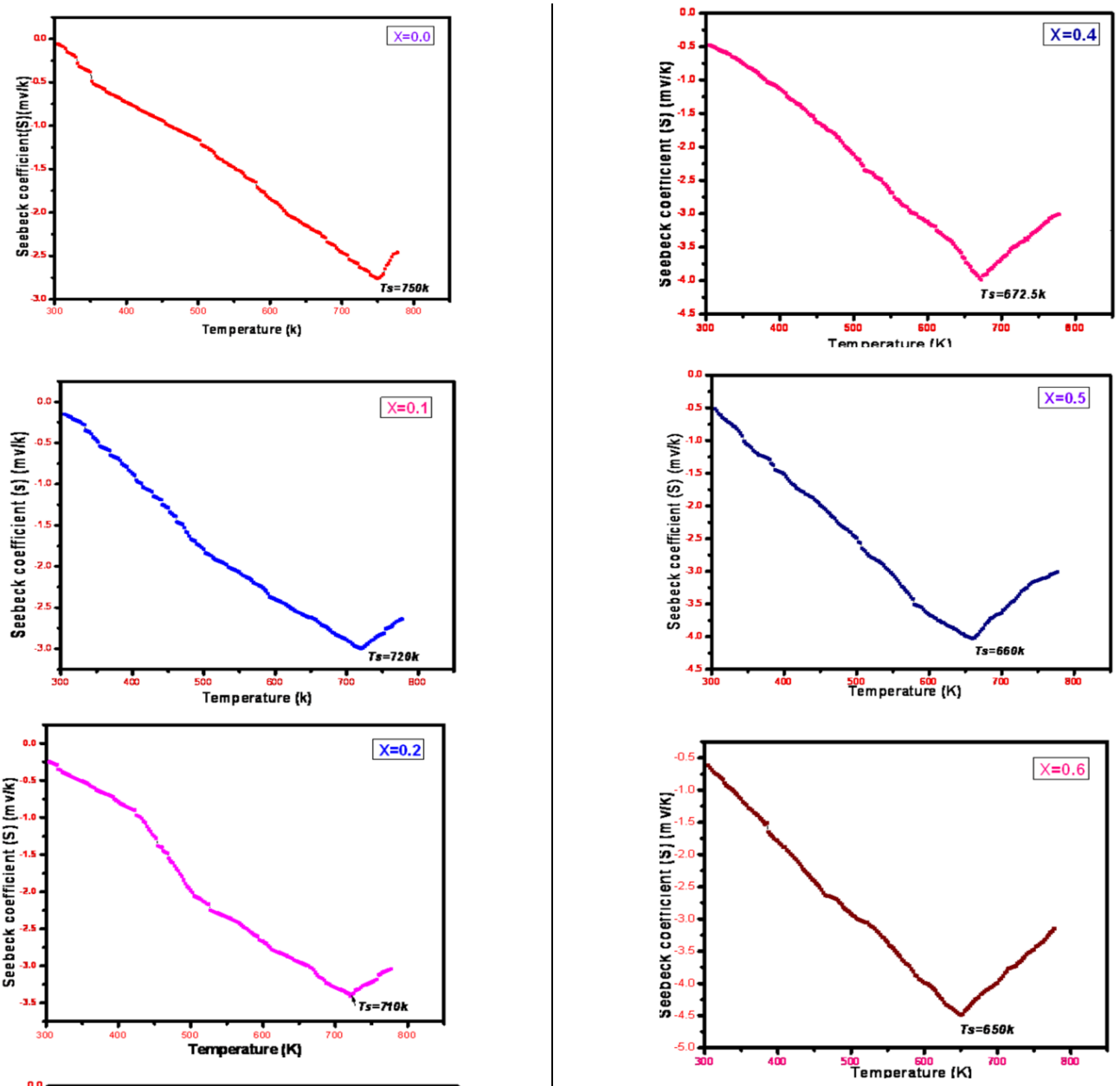

Figure 12. Variation of Seebeck coefficient with Temperature (K) of $Cd_xCo_{1-x}Fe_2O_4$ (x=0- 0.6)

4. CONCLUSIONS

Citrate-Gel Autocombustion technique was used to synthesize CCF nano particle. The conventional heating at 500C° made formation of single phase cubic spinel structure reflections of synthesized samples. The crystalline size of the synthesized Co-Cd ferrites nanoparticle is found in the range of 11 to17 nm. The lattice constants were increased with the increase of Cd-content in Co-Cd ferrites. The morphology of synthesized CCF systems analyzed using SEM and TEM. The pictures showed agglomeration between the particles sample with homogeneous grains in similar nature. The EDS spectra show the presence of Co, Cd, Fe and O without impurities and hence the spectra indicate the purity of the samples. The TEM pictures reveal the agglomerated nanoparticles of particle size changing from 12 to 68 nm. The FTIR spectra of the ferrite samples confirm the formation of cubic spinel. The variation of dc conductivity with temperature for all Co-Cd ferrite samples is seen using the Arrhenius plots. The increase of conductivity with increases intemperature confirms the magnetic semiconducting behavior of nanoferrites. The Seebeck coefficient of the prepared Co-Cd ferrite samples is increased with an increase in temperature. The Curie transition temperature of the samples was observed to be decreased with increasing Cd-content in the CCF ferrite. At low temperature of 300 K, the samples express the p-type semiconducting nature due to having +ve value of 'S' while the same shows –ve value at high temperature suggesting the n-type semiconducting behavior.

5. REFERENCES

1. Ahmad, R.; Gul, I.H.; Zarrar, M.; Anwar, H.; Bilal, M.K.N.; Khan, A. Improved Electrical Properties of Cadmium Substituted Cobalt Ferrites Nano-particles for Microwave Application. *Journal of Magnetism and Magnetic Materials* **2016**, *405*, 28-35, https://doi.org/10.1016/j.jmmm.2015.12.019.
2. Manohar, A.; Krishnamoorthy, C.; Chandra,K.; Babu, N. Dielectric, Magnetic hyperthermia and PhotocatalyticProperties of $ZnFe_2O_4$ Nanoparticles Synthesized by Solvothermal Reflux method. *Applied Physics A* **2019**, *125,* 477, https://doi.org/10.1007/s00339-019-2760-0
3. Ramaprasad, T.; Kumar, R.J.; Naresh, U.; Prakash, M.; Kothandan, D.; Naidu, K.C.B. Effect of pH Value on Structural and Magnetic Properties of $CuFe_2O_4$ Nanoparticles Synthesized by Low Temperature Hydrothermal Technique.*Materials Research Express* **2017**, *4*, 96-98, https://doi.org/10.1088/2053-1591/aad860.
4. Kumar, N.S.; Suvarna, R.P.; Naidu, K.C.B.; Kumar, G.R.; Ramesh,S. Structural and functional properties of sol-gel synthesized and microwave heated Pb0.8Co0.2-zLazTiO3 (z = 0.05–0.2) nanoparticles. *Ceramics International* **2018**, *44*, 19408-19420, http://dx.doi.org/10.1016/j.ceramint.2018.07.176.
5. Kumar, N.S.; Suvarna, R.P.; Naidu, K.C.B. Sol-Gel Synthesized and Microwave Heated Pb0.8-yLayCo0.2TiO3 (y= 0.2–0.8) Nanoparticles: Structural, Morphological and Dielectric Properties. *Ceramics International* **2018**, *44*, 18189-18199, https://doi.org/10.1016/j.ceramint.2018.07.027.
6. Boda, N.; Boda, G.; Naidu, K.C.B.; Srinivas, M.; Batoo, K.M.; Ravinder, D.; Reddy, A.P.; Effect of Rare Earth Elements on Low Temperature Magnetic Properties of Ni and Co-Ferrite Nanoparticles. *Journal of Magnetism and Magnetic Materials* **2019**, *473*, 228-235, https://doi.org/10.1016/j.jmmm.2018.10.023.
7. Hashim, M.; Raghasudha, M.; Shah, J.; Shirsath, S.E.; Ravinder, D.; Kumar, S.; Meena, S.S.; Bhatt, P.; Alimuddin, R.K.; Kotnala, R.K. High temperature dielectric studies of indium-substituted NiCuZn nanoferrites. *Journal of Physics and Chemistry of Solids* **2018**, *112,* 29-36, https://doi.org/10.1016/j.jpcs.2017.08.022.
8. Naresh, U.; Kumar, R.J.; Naidu, K.C.B. Optical, Magnetic and Ferroelectric Properties of $Ba_{0.2}Cu_{0.8-x}La_xFe_2O_4$ (x = 0.2 - 0.6) Nanoparticles. *Ceramics International* **2019**, *45*, 7515-7523,https://doi.org/10.1016/j.ceramint.2019.01.044.
9. Naresh, U.; Kumar, R.J.; Chandra, K.; Naidu, B. Hydrothermal synthesis of barium copper ferrite nanoparticles: Nanofiber formation, optical, and magnetic properties. *Materials Chemistry and Physics* **2019**, *236*, 121807, https://doi.org/10.1016/j.matchemphys.2019.121807.
10. Pubby, K.; Meena, S.S.; Yusuf, S.M.; Narang, S.B. Cobalt substituted nickel ferrites via Pechini's sol–gel citrate route: X-band electromagnetic characterization.*Journal of Magnetism and Magnetic Materials* **2018**, *466*, 430-445, https://doi.org/10.1016/j.jmmm.2018.07.038.
11. Kumar, N.S.; Suvarna, R.P.; Naidu, K.C.B. Grain and grain boundary conduction mechanism in sol-gel synthesized and microwave heated $Pb_{0.8-y}La_yCo_{0.2}TiO_3$ (y = 0.2-0.8) nanofibers. *Materials Chemistry and Physics* **2019**, *223*, 241-248,http://dx.doi.org/10.1016/j.matchemphys.2018.11.004.
12. Raghasudha, M.; Ravinder, D.; Veerasomaiah, P. Thermoelectric power studies of Co–Cr nano ferrites. *Journal of Alloys and Compounds* **2014**, *604*, 276–280, https://doi.org/10.1016/j.jallcom.2014.03.097.
13. Janrao, P.S.; Maurya, J.C.; Bhoraskar, S.V.; Mathe, V.L. Magnetic Field Sensor Based On Zn Doped Cobalt Ferrites Synthesized by Chemical Co-Precipitation Route, Proceedings of the 2015 2nd International Symposium on Physics and Technology of Sensors,8-10th March, Pune, India, 2015;pp. 159-161, https://doi.org/10.1109/ISPTS.2015.7220103.
14. Cullity, B.D. *Elements of X-ray diffraction.* 2nd ed. (Addison-Wesley, Reading, MA, 1978.
15. Vegard, L. The Constitution of Mixed Crystals and the Space Occupied by Atoms. *Z. Physik* **1921**, *5*, 17-23.
16. Naidu, K.C.B.; Kiran, S.R.; Madhuri, W. Microwave Processed NiMgZn Ferrites for Electromagnetic Interference Shielding Applications. *IEEE Transactions on Magnetics* **2017**, *53*, 2900207, http://dx.doi.org/10.1109/TMAG.2016.2625773.
17. Verwey, E.J.;Haayman, P.W.; Romeijn, F.C. Physical Properties and Cation arrangement of Oxides with Spinel Structures II. Electronic Conductivity. *J. Chem. Phys*. **1948**, *15*, 181, https://doi.org/10.1063/1.1746466.
18. Naidu, K.C.B.; Reddy, V.N.; Sarmash,T.S.; Kothandan, D.; Subbarao, T.; Kumar, N.S. Structural, morphological, electrical, impedance and ferroelectric properties of BaO-ZnO-TiO2 ternary system.*J Aust Ceram Soc* **2019**, *55*, 201-218,https://doi.org/10.1007/s41779-018-0225-0.
19. Raghuram, N.; Rao, T.S.; Naidu, K.C.B. Investigations on Functional Properties of Hydrothermally Synthesized $Ba_{1-x}Sr_xFe_{12}O_{19}$ (x = 0.0 - 0.8) Nanoparticles. Material Science in Semiconductor Processing **2019**, *94,* 136-150, https://doi.org/10.1016/j.mssp.2019.01.037.
20. Sivakumar, D.; Naidu, K.C.B.; Rafi, M.M.; Sathyaseelan, B.; Nazeer, K.P.; Begam, A.A. Structural and dielectric properties of superparamagnetic iron oxide nanoparticles (SPIONS) stabilized by sugar solutions. *Materials Science-Poland* **2018**, *36,* 123-133, https://doi.org/10.1515/msp-2018-0017.

21. Naidu, K.C.B.; Madhuri, W. Ceramic nanoparticle synthesis at lower temperatures for LTCC and MMIC technology.*IEEE Transactions on Magnetics* **2018**, *54*, 2300808, http://dx.doi.org/10.1109/TMAG.2018.2855663.
22. Chavan, P.; Naik, L.R.; Belavi, P.B.; Chavan, G.; Ramesha, C.K.; Kotnala, R.K. Studies on Electrical and Magnetic Properties of Mg-Substituted Nickel Ferrites.*Journal of ElecMateri* **2017**, *46*, 188, https://doi.org/10.1007/s11664-016-4886-6.
23. Naidu, K.C.B.; Madhuri, W. Effect of non-magnetic Zn^{2+} cations on initial permeability of microwave treated NiMg ferrites. *International Journal of Applied Ceramic Technology* **2016**, *13*, 1090-1095, https://doi.org/10.1111/ijac.12571.
24. Kumar, G.R.; Basha, D.B.; K. Naidu, K.C.B.; Ramesh, S.; Srinivas, K. Spectroscopic Properties of NiO, PbO, CaO and MgO Ionic Crystals Synthesized by Ball Milling. *Method. Recent Patents on Materials Science* **2019**, *11*, 1-12, https://doi.org/10.2174/1874464812666181122093655.

6. ACKNOWLEDGEMENTS

The authors are very grateful to Prof. J. Shiva Kumar, Head, Department of Physics, University college of Science, Osmania University, Hyderabad. One of the authors **Nehru Boda** is very thankful to **UGC, BSR-section** New Delhi, for their financial assistance. The authors also thankful to UPE-UGC-OU and DST-PURSE-OU.